

AN HEURISTIC MODEL OF PAPER RUPTURE

Benjamin C. Donner
Paper Physics & Mechanics Team
Weyerhaeuser Pulp, Paper, and Packaging R&D
Tacoma WA 98477 USA
donnerb@wdni.com

ABSTRACT

In-plane (Mode I) fracture of paper is tested at both cryogenic and standard temperatures. It is shown that newsprint tested at cryogenic temperatures is very nearly linear elastic but does not obey classical linear elastic fracture mechanics (LEFM). The discrepancy is traced to changes in the crack tip stress field due to the sheet's fibrous structure.

A new fracture model is proposed which integrates the Griffith energy method, Irwin's correction for nonlinear material behavior, and a similar correction for the fibrous structure. The statistical distribution of mass and local fibre orientation (structural formation) are explicitly considered, and the model thereby links fracture and tensile strength of paper. This approach is consistent with Bazant's theoretical treatment of quasi-brittle fracture.

The separation of material nonlinearity and structural formation permits:

- computing the Essential Work, linking the model to an established approach
- estimating the fast fracture response that might occur in practice
- normalizing strength for the paper machine dependent structural formation

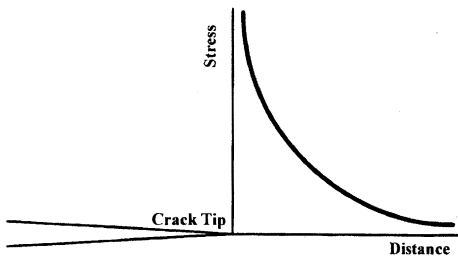
INTRODUCTION

The research described in this paper examined the reinforcement problem in paper. The commercial aspect of this problem addresses the cost/benefit of adding long, strong (and relatively expensive) kraft fibre to a weaker furnish as a means of improving runnability. The scope is somewhat narrower here, examining only the strength advantage of adding kraft fibre to TMP, and only considers dry newsprint webs. The influence of deformation *rate* on strength, ductility, and fracture resistance is considered directly.

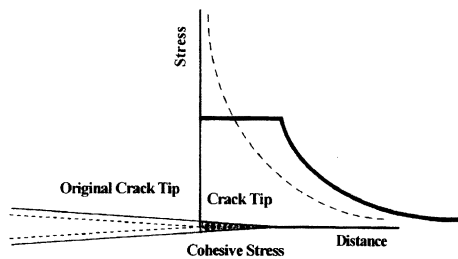
The starting point of this analysis is the energy balance first considered by Griffith (1). Griffith sought to explain the difference between measured and theoretical strength of engineering materials. This strength difference was found to be due to the influence of cracks and flaws. This was demonstrated using a linear elastic material under homogeneous tension as an ideal case.

Crack growth consumes energy. In Griffith's ideal material, the energy is consumed creating new surface area. This energy needs to be provided by the release of energy stored in the stressed material; this occurs as the crack grows. The Griffith criterion for crack instability is that the energy released by the material as the crack grows is equal to the energy consumed in creating new surface.

Griffith successfully applied this energy criterion to glass. In contrast, the stress-based analysis by Inglis (2) suggests that cracks induce a stress singularity (infinite stress) at the crack tip — cracked bodies should have no strength. This is shown in Figure 1a. The two approaches were reconciled by Savin (3). As the crack opens, cohesive stresses exist between the opening surfaces, until the crack surfaces reaches a critical separation. The maximum crack tip stress is reduced, altering the distribution of stress ahead of the crack from that derived by Inglis (Figure 1b). The Savin model shows that cracked bodies in fact have finite strength as expected. Further, Savin derives the Griffith energy criterion from the stress analysis, showing the two approaches to be consistent.



(a) Inglis stress field



(b) Savin stress field

Figure 1. Crack tip stress fields arising from uniform stress applied far from the crack.

Paper, as with most other engineering materials, does not have the ideal linear elastic mechanical behavior modeled by Griffith, Inglis, and Savin. Away from the crack, viscoelastic and plastic deformations absorb energy, making the energy unavailable to propagate the crack. Variations in fibre orientation, moisture, and temperature make the stress field inhomogeneous. Near the crack tip, the material nonlinearity interacts with the relatively high stresses and increases the unrecoverable energy absorption. Along with the local fibre structure, this redistributes the local stresses from that described by Inglis.

The presence of nonideal material behavior and structure should not alter the conceptual aspect of Griffith's criterion: crack growth will initiate when the energy released by the stressed body as the crack grows is just balanced by energy absorbed to create new crack surface. This should be true independent of the mechanism of energy absorption.

Balodis (4) and Andersson and Falk (5) have demonstrated that a direct application of Griffith's equation to paper does not work without additional consideration and modification. This was anticipated by Nissan (6) and others.

Bazant (7) theoretically derived a family of forms that express the energy criterion for crack instability in quasi-brittle materials. Quasi-brittle materials include paper, wood, and concrete, and can exhibit three types of departure from Griffith's ideal material: diffuse cracking, visco-plastic energy absorption and local stress variations due to microstructure. The simplest form of this family adds a virtual length to the actual length of the mechanical crack in Griffith's equation, in a way identical to Irwin (8).

Irwin applied the modified form of the Griffith equation to zinc foil, which exhibits crack tip plasticity. The virtual crack length extension effectively accounts for the modification of the crack tip stress field due to the plastic deformation. Andersson and Falk successfully applied the Griffith-Irwin equation to paper. They claimed in (5) that the virtual crack extension accounted for the influence of fibre structure, but clearly, material nonlinearity must have had an influence as well. Importantly, the aggregate effect of inelastic material and structural influences was captured by the Griffith-Irwin equation. That this is more than a regression fit to experimental data is strongly supported by Bazant's analysis.

Griffith-Irwin only handles the influence of material nonlinearity on the stress field near the crack tip. Global inelastic energy absorption requires separate consideration.

Figure 2 is a schematic of the stress-strain behavior of paper in loading, unloading, and reloading. The area under a stress-strain curve is the work per unit volume done on the material, so the total work done to load the sample is the area OAD. On unloading, only some of this work is recovered — that is, the

area ADB. Reloading generally takes much less energy (BCD) than the initial loading; this is because some of the work OAD goes into plastic deformation. This plasticity mechanism does not reactivate substantially until the highest load A is reached again at C.

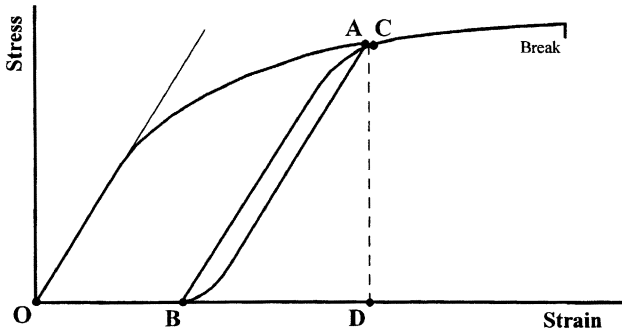


Figure 2. Typical stress-strain response of paper during loading, unloading, and reloading.

The reloading work is higher than the work recovered in unloading; the difference is the area of the hysteresis loop ABC. The area of the loop depends on the viscoelastic deformation of the material, and is therefore sensitive to the rate of loading. The initial slope E of the stress-strain curve is also sensitive to load rate; E is not a true material modulus at all owing to the component of viscoelastic relaxation, but nevertheless represents the initial rate of loading and unloading at a given deformation rate. Load cycling or “pre-stressing” the material suppresses plastic deformation on reloading, thereby extending the apparent linear region (compare OA to BA in Figure 2). At standard conditions, the viscous response of the material means there is no truly linear elastic region at all.

Inglis and Griffith assumed that the existence of the crack creates a local perturbation in the global stress field. Retaining that assumption, the

recoverable energy (ADB in Figure 2) can be estimated as σ_A^2/E . This estimate is used by Swinehart and Broek (9), Balodis and others. The effectiveness of this approximation depends on the rate of unloading relative to loading. The unloading rate can change both the unloading slope and the amount of viscoelastic recovery. These differences should normally be small compared to the total stored energy.

Pankonin and Habeger (10) used a compilation of research results and literature data to show that cryogenic temperatures effectively suppress the time-dependent viscoelastic behavior in paper. In the absence of the viscoelastic mechanism, the energy recoverable during fracture should be exactly σ_A^2/E . Time-independent plasticity may still take place at cryogenic temperatures, but this should not influence the recoverable energy.

Certain restraint-dried papers, such as the newsprint tested, are very nearly linear elastic at cryogenic temperatures. Testing the fracture behavior of paper at cryogenic temperatures ("cold") isolates the influence of the fibre structure. Retesting the same materials at standard conditions ("warm") after testing the cold behavior allows one to infer the role of viscoelasticity by itself.

Other paper types, such as cross-machine direction (CD) bond, exhibit marked nonlinearity of the cold stress-strain curve. The degree of this nonlinearity is substantially less than in warm tests, and is virtually time-independent. Phenomenologically, this is consistent with "plasticity" in the sample, but seems most likely to be caused by diffuse damage to the microstructure in the sense of Dougill (11). Further work will be necessary to demonstrate a bond or partial bond rupture described by Corte (12), Yamauchi *et al.* (13), and Page *et al.* (14), perhaps using similar acoustic emission measurements to those in (12-14).

A modified form of the Griffith equation is presented which separately identifies the influence of structure and material nonlinearity, in the spirit of Andersson and Falk, Irwin, and Bažant. These influences are determined in an experimental program measuring the fracture behavior of paper both at standard and cryogenic temperatures. Identifying the roles of structure and material separately contributes directly to our understanding of how reinforcing ("carrier") fibres increase fracture resistance and thereby improve dry web runnability.

EXPERIMENTAL METHOD

A. Testing Machine and Special Fixturing

Tensile and fracture testing was carried out on one inch (25.4 mm) test strips 160 mm long. Strips were clamped in novel fixturing, mounted on an MTS 850 servohydraulic test system, with ram speeds to 1.0 ms^{-1} . Load cell dynamics and inertial effects limit the quality of the data above 0.1 ms^{-1} . Slowest testing rates were limited only by the patience of the observer and the ability to measure minute displacements.

Figure 3 shows a schematic of the fixture. The upper clamp connects through a pair of rods to the load cell. The lower clamp is mounted on the frame of the test machine using rods of the same diameter as the upper clamp.

The clamps and rods are all made from Invar[®], a high nickel alloy with very low coefficient of thermal expansion, about one-eighth that of carbon steel ($0.8 \text{ vs. } 6.0 \times 10^{-6}/^{\circ}\text{C}$). This minimizes the dimensional changes in the fixture when immersed in liquid nitrogen (LN_2).

Once immersed in the nitrogen and at thermal equilibrium, variations in the LN_2 level will cause the rods to both the upper and lower clamps to change length. Since the two pairs of rods are identical in cross-section, the temperature profile in both rod pairs above the LN_2 will be the same. Any change in length will be the same for both rod pairs, so the clamps will not change relative position and the sample will not be deformed. No change in the measured load in the test strip due to thermal transients was detected, indicating the effectiveness of this arrangement. On initial cooling, the roughly 3% thermal shrinkage of the sample needed to be considered.

The same fixture was used for both cold and warm tests.

Ten specimens were tested at each crack size. Occasionally samples broke at the clamps. These were replaced with an additional specimen.

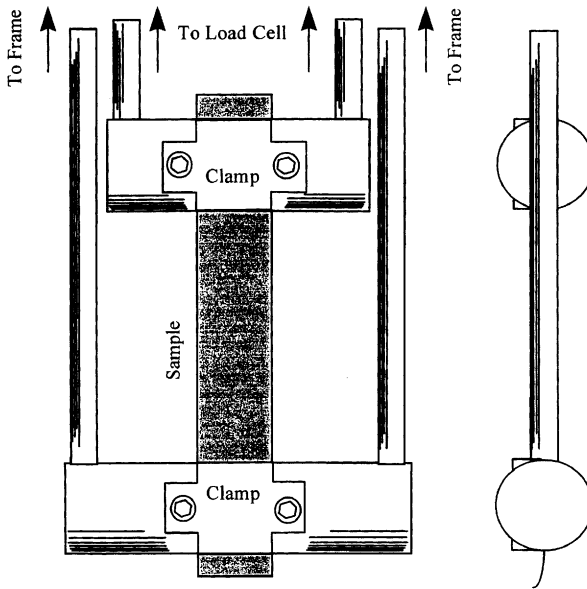


Figure 3. Cryofracture test fixture.

B. Mechanical Crack Insertion

Center slits were inserted by punching pieces of double ground razor blades (American Safety Razor Company, Gem®/Star®) through single samples. The razor blades were ground to width, with the vertical edges deburred to prevent microscopic tearing at the crack tips (Figure 4a).

Edge slits were inserted using the same double ground blades, but unaltered. A new blade was used for each cut. Ten strips were clamped between two steel plates (Figure 4b). The plates have a series of grooves of depths 1/4, 1/2, 1, 2, 4, 6 and 8 mm. The fixturing ensured that the two edge cuts were colinear,

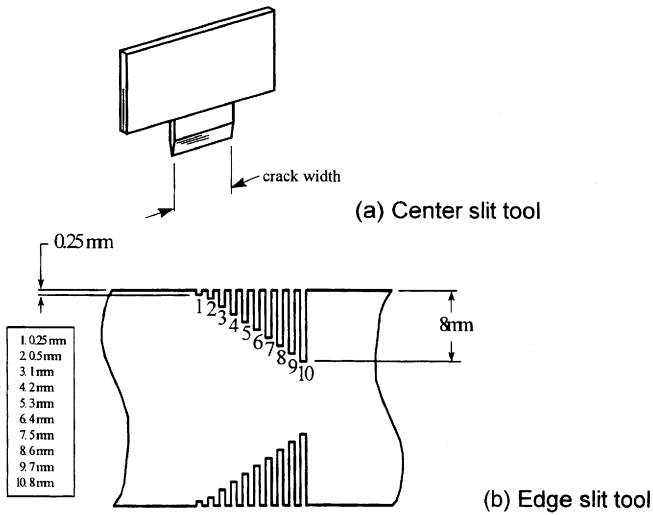


Figure 4. Center slit cutting tool (a) and edge slit template (b)

perpendicular to the strip centerline, and reproducible in length. The sharp edge of the blade forms the crack tip in this arrangement, so crack tip tearing was not an issue.

C. Data Acquisition

The MTS 458.20 controller uses analog amplifiers with a 1 kHz rolloff frequency. Data acquisition rates were 1 Hz-1 MHz using a Rapid Systems R1200, depending on the deformation rate. Over sampling made it possible to identify and filter high frequency instrumentation noise.

D. Measurement of Structural Formation

The term “structural formation” is used to capture the idea that local strength is being controlled by more than local mass (“formation”). Local fibre orientation is

a key contribution. The “intensity” of structural formation is assessed for purposes here as the pooled coefficient of variation in the strength tests (tensile and fracture). The fracture test conveniently defines the length scale, permitting direct computation of strength as a function of sample area (weak link effect).

FRACTURE MODEL DEVELOPMENT

A. Background

Inglis (2) determined the stress field around an elliptical hole. Given the major and minor axes as a and b respectively, Inglis sought to model a crack by shrinking the minor axis b to zero. Under the influence of uniaxial tensile stress σ_∞ applied perpendicular to the major axis, Inglis computed the stress at the ends of the ellipse as:

$$\sigma_{\max} = \sigma_\infty \left(1 + \frac{2a}{b} \right) \quad (1)$$

Although cracks may not have an elliptical form, Inglis goes on to show that σ_{\max} will be controlled by the crack tip radius. Computations of σ_{\max} can then proceed as though the crack were elliptical in form, under certain restrictions about crack tip smoothness.

Use of Eq. (1) to determine the residual strength of a cracked body requires geometric details of the crack tip. Griffith (1) found material strengths were underpredicted even for realistic assumptions about crack geometry. Griffith's energy argument was much more successful for brittle materials. The critical condition where a crack can just start to grow is where the potential energy released by the increased crack length is just balanced by the energy consumed in creating new surface. Given a critical nominal stress σ_c applied far from the crack, the energy to create new surface, γ , and (isotropic) elastic modulus E , Griffith determined that:

$$\sigma_c = \sqrt{\frac{2E\gamma}{\pi a}} \quad (2)$$

The Griffith criterion Eq. (2) can be applied to inelastic bodies under certain circumstances but the energy consumed in propagating the crack will be larger than 2γ . Given an energy release rate per unit crack extension per unit thickness, G :

$$\sigma_c = \sqrt{\frac{EG}{\pi a}} \quad (3)$$

$G \geq 2\gamma$ represents the energy cost of incrementally propagating a crack and is equivalent to the fracture resistance. This must be the combined effect of creating new surface and absorbing energy by the material in the fracture process zone (FPZ). When the material is in fact linear elastic, then $G=2\gamma$. An implied assumption underlying Eq. (3) is that the FPZ is small compared to the half crack length a . If there is a large FPZ involving plasticity, a modification of the Griffith approach is required.

A basic problem in finding G for cases with a large FPZ is that the elastic stress field solution forming the basis for the computation is itself influenced by the existence of the fracture process zone. Irwin (8) treated crack tip plasticity in the context of the elasticity solution by relocating the $1/\sqrt{r}$ singularity away from the crack tip, and then extending the crack to meet the new origin. This is shown in Figure 5.

Irwin's elastic-perfectly plastic material model implies that the stress is uniform throughout the plastic zone. By moving the origin from the tip of the physical crack to the center of the plastic zone, the stress "cut" from the singularity is just balanced by stress in the plastic zone to the left of the origin. Equilibrium is satisfied.

Using the Irwin correction to the physical crack length "a" gives a modified form of the Griffith equation:

$$\sigma_c = \sqrt{\frac{EG}{\pi(a + \delta a)}} \quad (4)$$

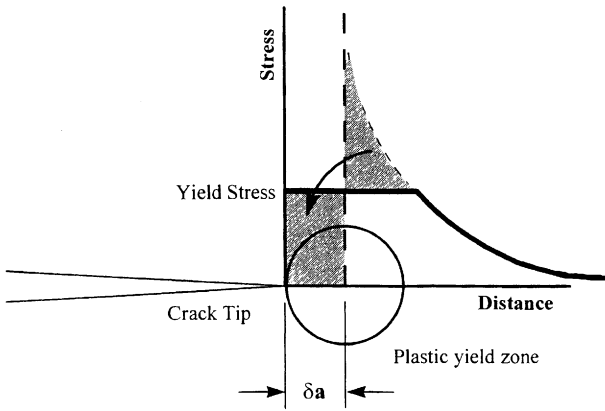


Figure 5. Irwin virtual crack extension preserving stress equilibrium.

G of course, reflects the energy absorption in the plastic zone, as well as the energy to create new surface.

Bažant (7) provides theoretical support for Irwin's choice. A careful investigation of possible consequences of structure led to a family of possible theoretical forms, of which the Irwin model Eq. (4) is the simplest. Bažant also argues that this family applies to all quasi-brittle materials, such as wood, concrete and paper. The structure of these materials gives rise to a rough fracture surface. The increase in surface area over a planar surface increases energy absorbed by the crack. This means the measured $G > 2\gamma$ for materials with microstructure, even if the material is linear elastic.

B. Crack Tip Stress Field

The Griffith Equations, Eqs. (2) and (3), and as modified by Irwin, Eq. (4), needs to be modified again to account for structural formation. In rewriting the form of the Eq. (4), the spirit of the original equation and the Irwin modification is kept,

but the contribution of *structure* to δa , δa_s , is separated from the contribution of *material nonlinearity*, δa_m :

$$\delta a = \delta a_m + \delta a_s \quad (5)$$

The additive separation is supported by Bažant (7).

Figure 6a represents a schematic view of how the structural formation represents a departure from the continuum assumption. Each crack tip will have a different distribution of stress due to differences in local fibre geometry and mass. Deconstructing due to fibre rupture and pull-out, described as thinning in (5), blunts the crack tip stress. Figure 6b shows how the nonlinear material properties influence the stress field, in a manner similar to Irwin's treatment. Figure 6c represents the combined effect of material nonlinearity and the fibrous structure.

The additive separation in Eq. (5) may be viewed as unrealistic, since structural formation will determine the local material properties. This interaction would mean δa_m is dependent on δa_s and the separation is incomplete. However, it will be demonstrated below that Eq. (5) is effective based on experimental results.

C. Weak Link Correction

The fracture initiation site in a tensile specimen will be determined by the local stress, grammage, and fibre orientation and can occur anywhere in the strip. In contrast, a fracture specimen (with sufficiently long cracks) fails by propagating the crack; the location is predetermined.

The average *material* strength in the fracture specimen will be higher than the average material strength in the tensile specimen, owing to the weak link effect. Of course, the nominal strength will typically be lower in the fracture specimen due to the crack.

The difference in material strengths of the fracture and tensile specimens is governed by the intensity of the structural formation, as exhibited by the *variation* in tensile or fracture strength. Since the material strength is governed by the

structural formation for both tensile and fracture strengths, it is presumed that the underlying distribution is the same for both cases. The pooled coefficient of variation for tensile and fracture tests is used in computing the weak link effect.

The radius of the fracture process zone δa defines the volume of material influencing crack tip strength. The volume of material in the tensile failure initiation site is like two adjacent FPZs. This is equivalent to the case of a zero length mechanical crack. The number of sites where tensile failure can occur, n , is related to the total tensile strip area $w \cdot l$ and to δa :

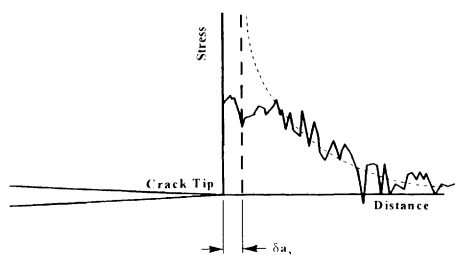
$$n = \frac{wl}{\pi \delta a^2} \quad (6)$$

where w is the strip width and l the length. Earlier work by the author (15, 16) used a three parameter Weibull distribution to determine the strength ratio for samples with area ratio n and coefficient of variation ξ to be:

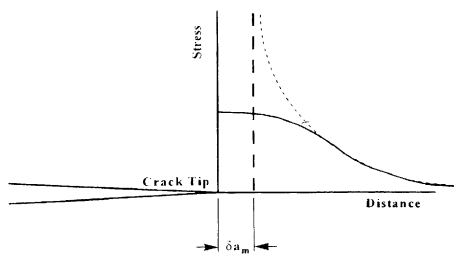
$$\frac{\bar{s}(n)}{\bar{s}(1)} = 1 - 3.24\xi(1 - n^{-0.2778}) \quad (7)$$

The zone of maximum stress ahead of the crack tip (Figure 6c) is roughly circular, with radius δa . The strength of this material, on average, is $\bar{s}(1)$. The tensile specimen has no such crack, but will break instead where the local strength is lowest, as determined by the structural formation.

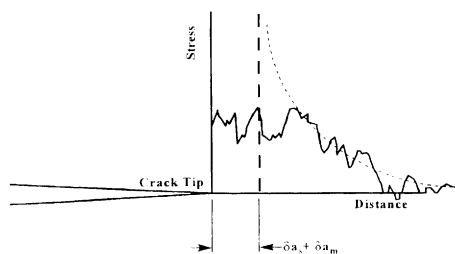
The tensile specimen is imagined to be composed of n local regions, the weakest of which is $\bar{s}(n)$, on average. The material strength $\bar{s}(1)$ was determined from the tensile strength $\bar{s}(n)$ by dividing by the weak link correction factor (WLCF). The WLCF is the right hand side of Eq. (7).



(a) Effect of structural formation



(b) Effect of material nonlinearity



(c) Combined effect

Figure 6. Structural and material effects on stress field.

D. Orthotropy Correction

Figure 7 represents an elliptical void with major axis "a" and minor axis "b". A uniform stress σ_∞ is applied far from the void. The stress is higher near the tips

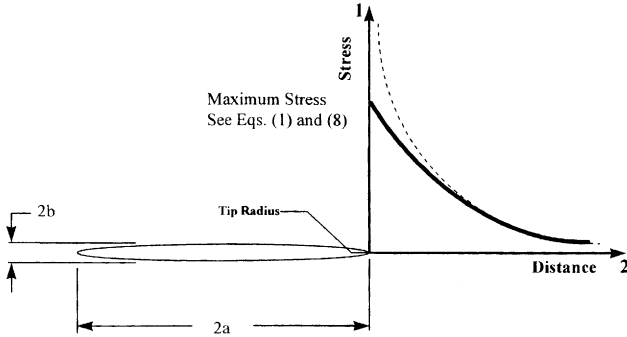


Figure 7. Elliptical Crack Stress Field.

of the ellipse due to the presence of the crack, and depends on the material properties. For an orthotropic elastic material, the maximum stress is:

$$\sigma = \sigma_\infty \left(1 + (\beta_1 + \beta_2) \frac{a}{b} \right) \quad (8)$$

where β_1 and β_2 are somewhat awkward functions of the orthotropic elastic moduli (3).

The in-plane shear modulus G_{12} can be approximated as (17):

$$G_{12} \approx \frac{\sqrt{E_1 E_2}}{2(1 + \sqrt{\nu_{12} \nu_{21}})} \quad (9)$$

where E_1, E_2 are the Young's moduli and ν_{12}, ν_{21} the Poisson's ratios in the plane of the sheet. Substitution of Eq. (9) in β_1 and β_2 in Eq. (8) shows the maximum stress at the tip of the void in Figure 7 to be a function only of the anisotropy ratio $R = E_1/E_2$:

$$\sigma \approx \sigma_\infty \left(1 + 2 \sqrt[4]{R} \frac{a}{b} \right) \quad (10)$$

The crack tip stress is highest when the "1" direction in Figure 7 is oriented along the fibres. In the isotropic case $R=1$, Eq. (10) reduces to Eq. (1).

Using the exact orthotropic correction given by Paris (18) and the approximation Eq. (10), it can be shown that the Griffith Eq. (2) is applicable to orthotropic materials if:

$$\frac{E_1}{\sqrt[4]{R}} \quad (11)$$

is substituted for E , where E , the Young's modulus is the direction of the applied stress.

E. Finite Width Correction Factor (FWCF)

The elasticity solution of the crack tip stress field is typically based on "infinite width" or periodic solutions. A correction whose form depends on sample geometry must be applied to account for the finite width of actual test specimens. These corrections are given in a number of sources, for example Broek (19). The corrections used here are:

$$\begin{array}{l} \text{Two Symmetric Edge} \\ \text{Cracks, each of length } a \end{array} \quad \text{FWCF}(a; w) = \frac{w}{\pi a} \tan\left(\frac{\pi a}{w}\right) \left\{ 1 + 0.122 \cos^4 \frac{\pi a}{w} \right\} \quad (12)$$

$$\begin{array}{l} \text{Central Crack of length } 2a \end{array} \quad \text{FWCF}(a; w) = \sec \frac{\pi a}{w} \quad (13)$$

F. Modified Griffith Equation

The final equation is a composite of the Griffith Eq. (2) and the various corrections described above:

$$\frac{\sigma_c}{f(a=0, \text{WLCF}(n; \xi, \delta a), 1)} = \sqrt{\frac{E_1 G_1}{4\sqrt{R} \pi (a + \delta a) \text{FWCF}(a + \delta a, w)}} \quad (14)$$

$$= f(a; G, \delta a)$$

where $\delta a = \delta a_s + \delta a_m$ after Eq. (5). The weak link correction is applied only to tensile specimens, when $a=0$. G_1 is the fracture resistance in the direction of the applied stress.

The substitution of the *corrected* half-crack length, $a+\delta a$, for a in the finite width correction factor is self consistent, since δa is structured so as to relate the actual case back to the ideal elasticity solution, and since the elasticity solution forms the basis for the computation of the FWCF.

G. Overlap of Strength Distributions

Examination of Eq. (14) in the limit $a \rightarrow 0$ shows a finite sample strength with no mechanical crack. This, of course, corresponds to the tensile strength of the specimen. Andersson and Falk (5) examined the significance of δa , concluding that this must be controlled by the underlying fibre structure.

A weak zone defined by adverse local fibre orientation and low grammage will concentrate stress in adjacent regions, analogous to a crack. For this reason, the intensity of the structural formation is represented by δa as an "equivalent crack size." See also the representation of flaws in Model Effectiveness.

So long as the mechanical crack length $a \gg \delta a$, the sample will break at the mechanical crack. If there is no mechanical crack, or the crack is much smaller than δa , the sample will break away from the crack and behave like a tensile specimen.

When the mechanical crack "a" is similar in size to δa , a particular sample may break either at the crack or away, depending on which is weaker. The fraction breaking "at" or "away" depends on the overlap of the distributions shown in Figure 8, and whether the weak side distribution A corresponds to fracture or tensile strength. This correspondence is determined from the relative frequency of breaking at the crack, η . If $\eta < 0.5$, then distribution B corresponds to fracture, but if $\eta > 0.5$ then A corresponds to fracture. At $\eta = 0.5$, the two distributions have the same mean.

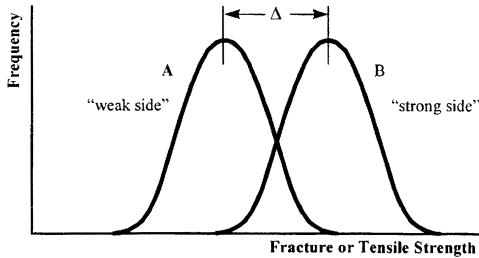


Figure 8. Overlapping probability density functions.

The underlying tensile strength and fracture strength distributions were modeled as symmetric three parameter Weibull, consistent with the weak link correction. The relative width of the distribution is given by the pooled coefficient of variation ξ . For a given experiment, the average strength \bar{s} and frequency η are known. The means μ_A and μ_B are not known, and need to be determined. This can be done using Table 1.

The table is symmetric in the fracture and tensile strength distributions. The relative fracture frequency η in the second column is the complement of the tensile failure frequency of $1-\eta$ given in the fourth. Estimates of the population mean μ are found from the measured average strength \bar{s} using the table. For example, if $\eta=0.3$, and the coefficient of variation $\xi=5\%$, then $\mu_T \approx \bar{s}_{\text{TENSILE}} = \bar{s}(1+0.2677 \cdot 0.05)$ and $\mu_F \approx \bar{s}_{\text{FRACTURE}} = \bar{s}(1+1.0219 \cdot 0.05)$.

	η	$(\mu_T/\bar{s}-1)/\xi$	$1-\eta$	$(\mu_T/\bar{s}-1)/\xi$	
No Overlap	0.0	-----	1.0	0.0000	No Overlap
B corresponds to Fracture	0.1	1.8922	0.9	0.0645	A corresponds to Fracture
	0.2	1.3624	0.8	0.1553	
	0.3	1.0219	0.7	0.2677	
	0.4	0.7865	0.6	0.4037	
A=B	0.5	0.5677	0.5	0.5677	A=B
A corresponds to Fracture	0.6	0.4037	0.4	0.7865	B corresponds to Fracture
	0.7	0.2677	0.3	1.0219	
	0.8	0.1553	0.2	1.3624	
	0.9	0.0645	0.1	1.8922	
	1.0	0.0000	0.0	-----	

Table 1. Correction to Average Strength arising from Tensile and Fracture Strength Distribution Overlap

H. Materials

Two commercial newsprints were compared. The newsprints were manufactured on different machines, and have somewhat different furnishes. The purpose of this testing was model evaluation, so both MD and CD fracture tests were conducted, both warm and cold. Data presented here is for double edge cracks; the results were consistent with center cracks and so the center crack results have been omitted.

Table 2 presents furnish and physical data for the two newsprints.

Sample	"A"	"B"
Density [kg/m ³]	626	674
Caliper[mm]	.0678	.0720
Grammage[g/m ²]	42.48	48.52
Furnish (TMP/Kraft/Deink+Broke)	51.1/16.1/32.8	49.6/0/50.4

Table 2. Furnish and Basic Properties

RESULTS

A. Cryogenic Stress-Strain Response

The demonstration that the MD newsprint exhibits linear elastic behavior is in two parts. Figure 9 shows a closed hysteresis loop at cryogenic temperatures, in contrast to the typical open (energy absorbing) loop at standard conditions. Measured plastic strain was 0.03% for both MD and CD when cold. Figure 10 shows stress-strain curves at five deformation rates warm and cold. The ultrasonic modulus is plotted for comparison. Increasing strain rate increases the initial slope of the stress-strain curve in the warm samples, showing the influence of viscoelasticity. The cold samples have nearly identical, straight-line stress-strain response, showing an absence of viscoelasticity, as expected from Pankonin and Habeger (10) and showing the absence of plasticity.

B. Model Effectiveness

Figure 11a shows the application of Eq. (14) Newsprint "A". The required constants G and δa are determined from a nonlinear regression of the data. In Figure 11a, the data were determined based on the average of the ten samples for each crack size. Similar results are obtained when individual data points are used in the regression. The data are the filled circles and the straight line is the linear regression through the strength data and the model, using the previously determined G and δa . Note the r^2 above 99%.

When δa is set to zero, emulating Griffith's Eq. (2), the result is not linear (solid triangles). Even though the cryogenic material properties are linear elastic, as required by Griffith, Eq. (2) is not effective. This failure is due to the underlying fibrous structure, as suggested by Andersson and Falk (5).

The consistency of tensile strength with the fracture model is shown in Figure 11b. The fracture data for crack sizes $2a = 0.5, 1, 2, 4, 8, 12$ mm were used in the regression. The tensile data was plotted using Eq. (14), the regression values for G and δa , and with $a=0$. The weak link correction factor has been applied. Although the tensile data were not part of the regression, the results are consistent with the fracture regression. This shows that the structural formation,

with virtual crack extension $2\delta a$, is responsible for tensile failure in a way self consistent with fracture at a mechanical crack. Hereafter, the tensile data were combined with the fracture data for determining G and δa by regression.

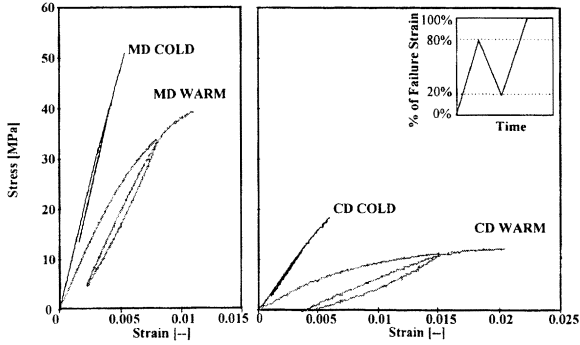


Figure 9. Mechanical Response to Load Reversal at Standard and Cryogenic Temperatures.

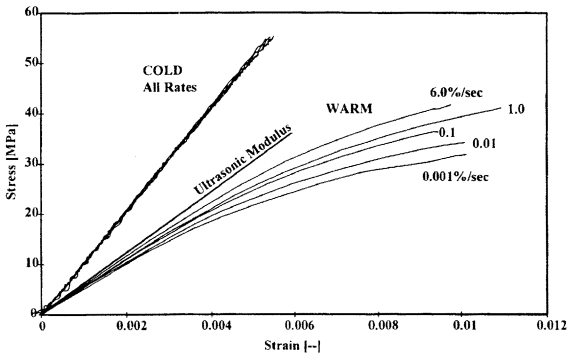
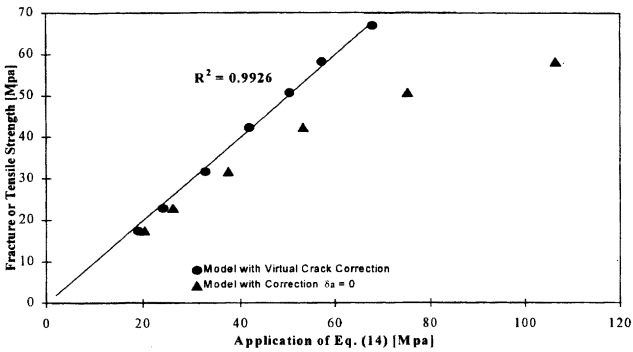
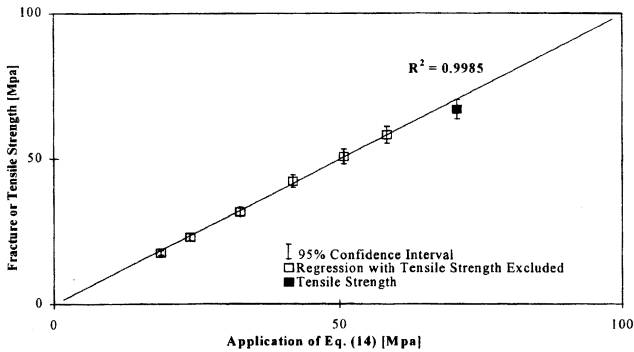


Figure 10. Mechanical Response to Changes in Strain Rate at Standard and Cryogenic Temperatures.

(a) Effect of setting virtual crack size $\delta a = 0$ 

(b) Tensile strength is consistent with fracture model

Figure 11. Model effectiveness.

An independent verification of flaw size can be made using the relative frequency that samples break at the crack η_f . For progressively smaller

mechanical cracks, more of the samples will break away from the crack. When half of the samples break at the crack, and half away ($\eta_F = 0.5$), the distributions are superposed. The size of the mechanical crack will be the same as the flaw size a_i causing the material to fail in a tensile test.

Two estimates can be made of the flaw size, a_i . Once G and δa are determined, direct application of Eq. (14) to tensile data (unmodified for the weak link effect) will permit solving for a_i . This requires solving

$$f(a_i; G, \delta a) - \sigma_T = 0 \quad (15)$$

for a_i , where σ_T is the tensile strength.

It has been argued previously that the tensile strength, divided by the WLCF, gives the average local material strength. This must be the same as the strength given by Eq. (14) with $a = 0$. Taking the ratio of Eq. (14) applied to the cases $a = a_i$ and $a = 0$ gives a second way to find a_i :

$$\frac{f(a_i; G, \delta a)}{f(0; G, \delta a)} = \frac{\sigma_T}{\sigma_T / WLCF(\eta; \xi, \delta a)} \quad (16)$$

which can be simplified to show

$$a_i \approx \frac{1 - WLCF(\eta; \xi, \delta a)^2}{WLCF(\eta; \xi, \delta a)^2} \cdot \delta a \quad (17)$$

The two measures of a_i given by Eq. (15) and (17) are independent.

Figure 12 confirms that $2a_i$ is the flaw equivalent crack size. This shows consistency between the regression results and the underlying statistical distribution of defects. It is also apparent that the flaw size a_i is similar in size to δa , at least in this case, linking the flaw concept to the structural formation.

Table 3 shows the regression results and physical test data for the cold fracture and cold tensile specimens. Table 4 contains the corresponding data for standard conditions at 0.67%/sec deformation rate.

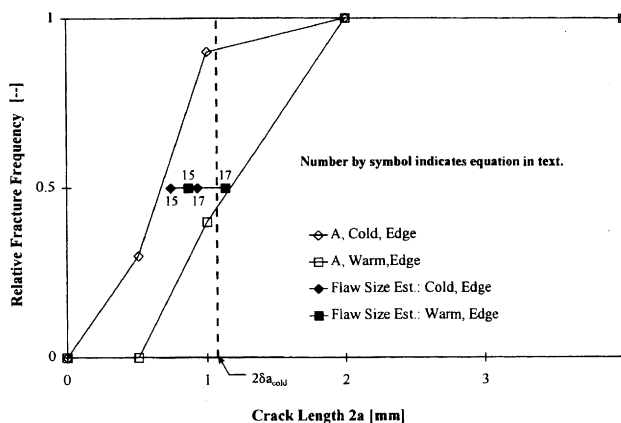


Figure 12. Fracture frequency plotted against crack length.

Sample:	"A" MD	"A" CD	"B" MD	"B" CD
Elastic Modulus E[GPa]	10.47	3.26	10.58	2.57
Tensile Strength [MPa]	51.67	16.95	57.56	15.20
Pooled COV, ξ	0.0788	0.0773	0.0833	0.0763
WLCF	0.7713	0.7879	0.7513	0.7873
Tensile Strength w/WLCF [MPa]	67.03	21.54	76.65	19.32
Tensile Index [Nm/g]	82.5	27.1	85.4	22.5
Failure Strain ϵ [%]	0.504	0.552	0.558	0.651
Fracture Resistance G [J/m ²]	1274	471	1015	373
G/ ρ [Jm/g]	2.04	0.75	1.51	0.55
δa [mm]	0.614	1.229	0.369	1.022
a_c [mm], calculated by Eq. (15)	0.464	0.880	0.254	0.620
a_c [mm], calculated by Eq. (17)	0.368	0.597	0.325	0.678

Table 3. Newsprint Fracture Data - Cold

Sample	"A" MD	"A" CD	"B" MD	"B" CD
Ultrasonic Modulus [GPa]	6.059	1.890	6.140	1.481
Elastic Modulus E[GPa]	5.52	1.29	5.42	1.01
Modulus Ratio, $R^{1/4}$	1.438	.695	1.522	.657
Tensile Strength [MPa]	39.84	11.81	40.23	10.86
Pooled COV, ξ	0.0526	0.0534	0.0463	0.0361
WLCF	0.8585	0.8764	0.8758	0.9156
Tensile Strength w/WLCF [MPa]	46.40	13.47	45.97	11.86
Tensile Index [Nm/g]	63.6	18.9	59.77	16.1
Dry Zero Span Index, Z [Nm/g]	131.2	56.4	122.7	51.8
Failure Strain, ϵ [%]	1.040	1.952	1.043	3.372
Fracture Resistance G [J/m ²]	2868	1408	3065	1206
G/ ρ [Jm/g]	4.58	2.25	4.55	1.79
δa [mm]	1.480	3.769	1.5157	3.601
a_i [mm], calculated by Eq. (15)	0.433	1.44	0.374	0.956
a_i [mm], calculated by Eq. (17)	0.566	0.857	0.492	0.546

Table 4. Newsprint Fracture Data - Warm

C. Essential Work

δa is the radius of the fracture process zone which exists at each crack tip (see Figure 5). For cryofracture, this is due to structure alone. Warm samples have a larger FPZ (and larger δa), due to viscoelastic, plastic, and structural effects. Since the underlying structural contribution $\delta a_{\text{cold}} = \delta a_s$ is known from the cold tests, the viscoelastic/plastic contribution is found from δa_{warm} by subtraction:

$$\begin{aligned}\delta a_s &= \delta a_{\text{structure}} = \delta a_{\text{cold}} \\ \delta a_m &= \delta a_{\text{material}} = \delta a_{\text{warm}} - \delta a_{\text{cold}}\end{aligned}\quad (18)$$

Eq. (18) can be used to identify the changes in fracture resistance from structural formation, fibre morphology, and bonding. This work is still in progress. Eq. (18) was used to demonstrate the relationship between the model in Eq. (14) and Essential Work of Fracture (EWF)(20). EWF is a fairly well established

technique for determining fracture resistance by testing a series of geometrically similar coupons of various size. A normalization and extrapolation are used to eliminate work required to deform the specimen but not involved in propagating the crack. The remaining energy is the work required to propagate the crack (essential work). Slow stable propagation of the crack is required to obtain the work of fracture.

Figure 13 shows a schematic of the slow fracture process utilized by EWF. Stable crack growth occurs and the nominal stress drops eventually to zero as the crack traverses the ligament (material remaining between the two edge slits). By using a constant ligament/width ratio of 1/3, the geometry corrections for finite width are constant. Plotting total area under the stress-strain curve in Figure 13 curve for various crack lengths and extrapolating to zero crack length gives the essential work. The essential work is the total work less the local and global geometry-dependent work due to material energy dissipation.

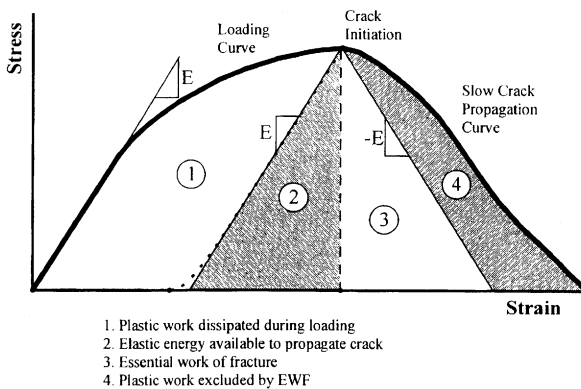


Figure 13. Stress-strain curve in slow fracture process.

The total work (per unit volume) done during the slow fracture process is the area under the stress-strain curve to the right of the initial crack propagation in Figure 13 (taken as the peak stress). Eliminating the plastic work ④ leaves the

essential work, the same as the elastic energy stored in the material at the peak stress σ_f . This area is σ_f^2/E , the square of the fracture strength (maximum stress in Figure 13) divided by the elastic modulus in the direction of the test.

An independent measure of EWF can be computed using Eq. (14) and the fracture resistance G given in Table 4 (warm data). However, since EWF eliminates the influence of plastic work in the fracture process zone, δa_{cold} must be substituted for δa_{warm} , after the manner of Eq. (18). This leaves in the influence of structure.

Table 5 shows a comparison between the measured and computed EWF. The reasonable comparison shows that the proposed model links back to this established technique. The advantage in the present technique is that fast fracture is used to find G at a considerable savings of laboratory time. The cryofracture technique adds insights about the role of structure not available from the EWF procedure.

Sample	A_{MD}	A_{CD}	B_{MD}	B_{CD}
EWF [Jm/kg]	16.2	12.2	14.6	9.9
Computed EWF [Jm/kg]	14.4	11.9	14.7	10.6
Difference [%]	-11	-2	+1	+7

Table 5. Essential Work of Fracture Comparison of EWF with Value Computed From Eq. (14)

DISCUSSION

The typical size of the correction $\delta a_{\text{structure}}$ is about 1 mm. The structural influence on fracture becomes small as the sample sizes and crack sizes increase since under these circumstances $a + \delta a \approx a$. The work by Gregersen, Fellers, *et al.* (21) addresses only the influence of material inelasticity, which is proper because of the large 1.0 x 0.5 m samples. At the other end of the spectrum the ultralight grammages studied in network mechanics and reviewed in (22, 23) are dominated by structural issues.

The comparison of cryofracture behavior of newsprint with standard condition testing at different rates reveals a change in relative importance of fibre bonding and fibre strength. Ranger (24) observed that the number of broken fibres increased with test rate, showing that fibre strength increases in importance with rate. At low deformation rates, or when the structure is moist, more fibres pull out, showing that fibre bonding is of increasing importance.

Figures 14 and 15 show MD tests of newsprint fractured at cryogenic and warm temperatures, respectively. Fibre fracture is dominant when cold (Figure 14). Fibre pullout is dominant when warm (Figure 15), with bonding and fibre length key attributes. These conclusions are supported by examining the relationship between tensile and fibre strengths. Using tensile strength σ_T and zero span strength Z given in Table 4, the ratio of these strengths is computed and given in Table 6. The weak-link correction factor WLCF has been applied to the tensile strength data.

$\frac{\sigma_f}{\text{WLCF} \cdot Z}$	Newsprint "A"	Newsprint "B"
WARM	0.56	0.56
COLD	0.82	0.93

Table 6. Relative Importance of Fibre Strength in Controlling Fracture and Tensile Strength

The relative importance of fibre strength in controlling the initiation of fracture — at a shive defect, say, depends on the rate, moisture, and temperature at which the material around the defect is stressed. This is equally true for the relative importance of structural formation: fibre strength is of increasing importance as stress rate increases, and as moisture and temperature decrease.

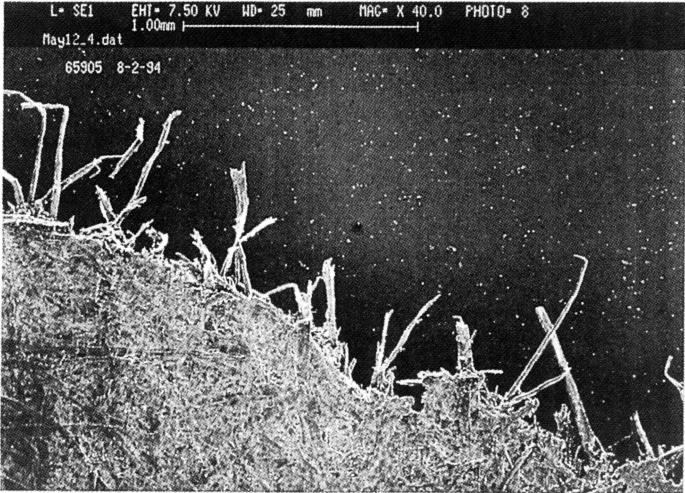


Figure 14. Newsprint Cryofracture scanning electron micrograph.

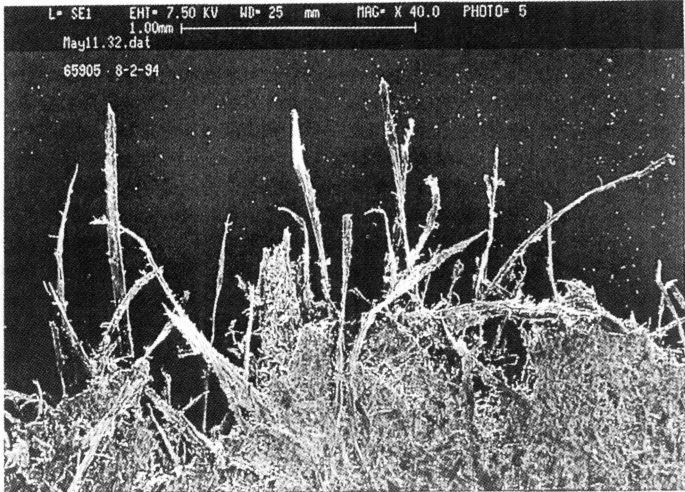


Figure 15. Newsprint Fracture at Standard Conditions.

CONCLUSIONS

- Tensile strength and fracture resistance of paper are related through both material properties and structural formation.
- Cryofracture and standard tests of fracture permit separating the material and structural influences on fracture and tensile behavior.
- Fast fracture of dry webs is dominated by fibre strength.

ACKNOWLEDGMENTS

I am indebted to Mr. John Unbehend and Mr. Dean Decrease for stable support during the development of the experimental procedure and modeling. Mr. Peter D. Cyr, Mr. Robert T. Peterson, Mr. Khanh Nguyen, and Ms. Shawna Brown are responsible for the meticulous laboratory work. Mr. William Herring, Dr. Curt Bronkhorst, and Dr. Keith Bennett are thanked for many contributions during model development. Mrs. Heide Nutwell is thanked for preparing the manuscript. Dr. Peter Ariessohn is thanked for detailed review of the manuscript.

REFERENCES

1. A. A. Griffith, "The Theory of Rupture," Proceedings, 1st International Conf. Applied Mechanics, Delft, 55-63, 1924.
2. E. Inglis, "Stresses in a Plate Due to the Presence of Cracks and Sharp Corner," Trans. Inst. Naval Arch., **55**, 219-230, 1913.
3. G. N. Savin, Stress Distribution Around Holes, NASA translation TT-F-607, 1965.
4. V. Balodis, "The Structure and Properties of Paper, Part XV. Fracture Energy," Aust. J. Appl. Sci., 283-304, 1963.
5. O. Andersson and O. Falk, "Spontaneous Crack Formation in Paper," Svensk Papperstidning **69** (4), 91-99, 1966.

6. A. H. Nissan, "General Principles of Adhesion, with Particular Reference to the Hydrogen Bond," in The Formation and Structure of Paper, Transactions of the British Paper and Board Maker's Assoc., F. Bolam, ed., I, 119-130, 1962.
7. Z. P. Bažant, "Scaling of Quasi-Brittle Fracture and the Fractal Question," J. Eng. Matls. and Techn. **117**, 361-367, October 1995.
8. G. R. Irwin, Handbuch der Physik, Hrsg. S. Flügge, VI, 551-590, 1958.
9. D. Swinehart and D. Broek, "Tenacity and Fracture Toughness of Paper and Board," JPPS **21** (11), J389-J397, November 1995.
10. B. Pankonin and C. Habeger, "A Strip Resonance Technique for Measuring the Ultrasonic Viscoelastic Parameters of Polymeric Sheets with Application to Cellulose," J. Polymer Sci: Part B: Polymer Physics, **26**, 339-352, 1988.
11. J. W. Dougill, "On Stable Progressively Fracturing Solids," J. Appl. Mathematics and Physics (ZAMP), **27**, 423-436, 1976.
12. H. Corte, "Faserstruktur und Physikalische Eigenschaften von Papier," Das Papier, **16**, 575-587, 1962.
13. T. Yamauchi, S. Okumura, and K. Murakami, "Measurement of Acoustic Emission during the Tensile Straining of Paper," JPPS, **15**(1), J23-J27, January, 1989.
14. D. H. Page, P. A. Tydeman, and M. Hunt, "Behavior of Fibre to Fibre Bonds in Sheets under Dynamic Conditions," in The Formation and Structure of Paper, F. Bolam ed., Transactions of the Technical Section, British Paper and Board Makers' Assoc., **1**, 249-264, 1962.
15. B. C. Donner, The Impact of Structural Formation on Compression Strength of Paper, Weyerhaeuser Internal Report, August 11, 1989.

16. B. C. Donner, Prediction of Linerboard Compression Strength in Box Sidewalls from Strip Compression Testing, Weyerhaeuser Internal Report, February 21, 1995.
17. R. Sziland, Theory and Analysis of Plates, Prentice-Hall, Inc., Englewood Cliffs, NJ, 1974. Cited and used by G. A. Baum, D. C. Brennan, and C. C. Habeger, "Orthotropic Elastic Constants of Paper," Tappi, **64**(8) , 97-100, 1981.
18. P. C. Paris and G. C. Sih, "Stress Analysis of Cracks," Fracture Toughness Testing and Its Applications, ASTM Special Technical Publication 381, 30, 1965.
19. D. Broek, Elementary Engineering Fracture Mechanics, Noordhoff Int'l. Publ., Leyden, 76, 1974.
20. R. S. Seth, "Measurement of In-Plane Fracture Toughness of Paper," TAPPI J., **78**(10) , 177-183, 1995.
21. O. Gregersen, C. Fellers, et al, "Application of Non-Linear Fracture Mechanics to Paper," Proceedings: Progress in Paper Physics - A Seminar, June 9-14, 1996, Stockholm, Sweden, 131-133, 1996.
22. K. Niskanen, "Strength and Fracture of Paper," in Products of Papermaking, Transaction of the Tenth Fundamental Research Symposium held at Oxford, C. F. Baker, ed.. PIRA Int'l., Leatherhead, **2**, 641-725.
23. C. T. J. Dodson and, P. T. Herdman, "Mechanical Properties of Paper," Chapter 7 in Handbook of Paper Science Vol. 2: The Structure and Physical Properties of Paper, Elsevier, New York, 71-126, 1982.
24. A. E. Ranger, Discussion in The Fundamental Properties of Paper Related to Its End Uses, Transactions of the Technical Div. British Paper and Board Makers' Assoc., F. Bolam, ed. , 302, 1976.

Transcription of Discussion

An Heuristic Model of Paper Rupture

Benjamin C Donner, Weyerhaeuser, USA

Professor Douglas Wahren

Thank you very much Benjamin. It is quite an interesting approach I think that may bridge some of the problems we have when trying to connect elastic and fracture properties.

Bryan Phillips Shotton Paper Co plc, UK

Thank you for that interesting approach. I have a feeling that fracture toughness is fundamentally flawed however, the reason being that the strain rates you are using in your apparatus are 0.1 metres per second while in applications in newsprint we are running at speeds which are at least 2 orders of magnitude higher than that. That means that the strain rates you are contemplating are of the order of 1-10 per second and the strain rates in practice as we have seen are 10^4 - 10^5 per second. Now that means that the thermodynamics are totally different in practice to what they are in lab experiments with fracture toughness machines. There is not time for the energy to redistribute around the fracture tip. Have you any comments to make on that, and can we possibly devise any instruments that will have a look at fracture toughness at realistic strain rates.

Benjamin Donner

Yes - there are several things. One, is that irrespective of the speed of the paper machine when the crack propagates, the crack propagates at the speed of sound in paper. That means that the rates are very well defined. It is wrong to assume that because the paper machine is running fast that the initiation is fast. We just do not know what the initiation strain rate is. While we cannot know that, we can know what the property change is going from laboratory rate to something that is very fast. Paper is not a linear viscoelastic solid, so Boltzmann's super position does not apply exactly. There is still a time temperature super position that applies. When I test cold, I am basically testing at a very high strain rate. The actual strain rate in the laboratory is quite small, but when I quench the viscoelasticity it is equivalent to testing at a very high rate at laboratory temperatures. So in essence we do have the information that you want: we have the change in the properties going from a very low test rate to a very high test rate. What we do not have is the information about the actual strain rate in the initiation phase, but we do know that it is much smaller than what is anticipated based on the speed of the process.

Bryan Phillips

High speed videos of fractures both on the papermachine and in the printing press do appear to show that propagation is very very fast.

Benjamin Donner

It is the speed of sound - it is defined it is a number.

Bryan Phillips

I take your word that it is also developing at the speed of sound in your apparatus.

Benjamin Donner

Yes that is right - that's physics. Wonderful subject.

Dr Raj S Seth, Paprican, Canada

I would like to comment on your "structural formation". There used to be a concept in polymers called the "inherent flaw". Are the two similar?

Benjamin Donner

There are inherent flaws in paper, and they are distributed in size - so there is a relationship of sorts. I am aware of this concept, and that it is phenomenological in the same way that the inherent flaws are. What is important in terms of structural formation is that we acknowledge explicitly the role of adverse fibre orientation in low basis weight and in terms of controlling the initiation, and that it is a stochastic process.

Raj Seth

I have a comment about Andersson and Falk's work. If I recall correctly, the structural flaw in a sheet of paper is quite large. In their work they used 1.5cm wide samples. Considering the size of the flaw, the size of the sample, 1.5cm does not make sense; it is too small. The other thing is they push their data through the origin to fit the Griffith relation, and calculate a correction factor. If you look at this now, particularly with their sample size, the entire treatment is questionable. I think we discussed this issue in our 1974 paper in the J. Mater. Sci.

Benjamin Donner

I anticipated the kind of comment you would make Raj. It is important to look back at Andersson and Falk's work and realise that it was not a complete perception of what happens in paper. They had no way of separating out the role of material and the role of flaw. However, that was 1965 and they stimulated the thinking around the role of structure, and then we abandoned it for 30 years! It is just that in the type of testing we are doing we are not considering structure, and I am asking us to do that now.

Raj Seth

It is good to learn from other materials also. There are materials that are full of stress concentrations or full of holes - ceramics and sintered metals are examples. Have you seen any similarity between what you are doing for paper and what they have done?

Benjamin Donner

The Bazant papers on quasi brittle materials discuss that in detail. There is considerable recent work on how distributed failures coalesce.

Mark T Kortschot, University of Toronto, Canada

If I understand it correctly the model involves adding together the actual flaw size the structural flaw size and the material based flaw size. I did not catch the numbers for newsprint but for regenerated cellulose the structural flaw size, obtained by extrapolation, was something that was very small. What was it for newsprint?

Benjamin Donner

The structural component was 0.6mm and then the total was 1.5mm.

Mark Kortschot

So you are adding the structural component to the actual crack length.

Benjamin Donner

Yes to make the virtual crack.

Mark Kortschot

The inherent flaw that we talk about is a physical thing which we obtain by extrapolation down to a tensile specimen. Don't we need to have that flaw at the tip of the crack to be able to add the two together?

Benjamin Donner

It does work and it does have meaning, but it does take careful consideration, and it is an area of continued interest. It is the area where the network mechanics model will play a role in elucidating exactly what happens at the tip of the crack in terms of the network.

Stuart Loewen, Associate - LSZ Papertech Inc, Canada

Unlike 20 years ago the tools now exist to rapidly quantify fibre orientation and basis weight variability on the scales that you are interested in and that you are claiming that your model is deconvolving from the contribution to the essential work of fracture so my question is - have you done this comparison between the residual essential work of fracture on those two newsprint samples and their variability? That would be an independent test of how well you are modelling those aspects.

Benjamin Donner

In the paper we do assess the structural formation directly by making strength variability assessments. Strength variability is the combined influence of the fibre orientation, basis weight, density, filler distribution, and the rest. That is the link that we are using to connect the model to essential work.